Investigating the effect of metal ions of different oxidation states (M^{x+}, x=1, 2, 3, & 4) on the PL emission of $Zn_4B_6O_{13}:Eu^{3+}$

ET Maleho, MLA Letswalo and BM Sondezi

Department of Physics, University of Johannesburg, 55 Beit St, Doornfontein, Johannesburg, 2028, South Africa.
E-mail: letswalom@uj.ac.za

Abstract. In this study, Eu^{3+} (fixed at 2 mol%) activated $Zn_4B_6O_{13}$ phosphors incorporated with metal ions of different oxidation states M^{x+} (x = 1 - 4) were successfully prepared by combustion synthesis method. The luminescence characteristics of $Zn_4B_6O_{13}:Eu^{3+}$ were improved by partially substituting metal ions for various oxidation states.. The crystal structure properties of the prepared materials were studied by X-ray diffraction (XRD), which revealed the formation of a zinc metaborate cubic crystal structure for all the samples. Surface features and the elemental analysis of the phosphor materials were studied by SEM and EDS, respectively. Excitation and emission scans were recorded for different metal ions. Upon excitation at 395 nm, the emission spectrum exhibited five distinct peaks at 580 nm, 592 nm, 614 nm, 653 nm, and 706 nm, corresponding to the $^5D_0 \rightarrow {}^7F_J$ (J = 0 - 4) transitions, confirming the presence of the Eu^{3+} ion. The optimal emission of the Eu^{3+} dopant into the $Zn_4B_6O_{13}$ host was of Bi^{3+} substitution, which resulted in the phosphor achieving an excellent PL intensity and a color purity of 91.16%. Tunable luminescence from the reddish-orange area (0.620, 0.355) of Commission Internationale de l'éclairage (CIE) towards the red area (0.641, 0.351) was achieved by substituting different oxidation states M^{x+} (x = 1 - 4). Therefore, different oxidation states M^{x+} (x = 1 - 4) and Eu^{3+} doped $Zn_4B_6O_{13}$ phosphor may be suitable candidates for the development of display devices and white light emitting diodes.

1 Introduction

At present, scientists' attention has been attracted by the rare earth ions activated luminescent materials due to their applications in various aspects [1, 2, 3]. Exploration of these materials has an advantage as they contribute to the improvement of material science research. One of the most important requirements for high performing materials is the selection of the host material in which the rare earth ions can be incorporated. One of the interesting applications of such materials is solid state lighting which is considered the next generation of lighting due to its attractive qualities such as low energy costs, long lifespan, and environmental friendliness [1, 4]. Many researchers have been exploring different borate materials as host lattices mainly because of their convenient properties such as large band gap, high thermal stability, low cost, and effective luminescence efficiency [5, 6, 7]. Amongst other borates, zinc metaborate with the chemical equation $Zn_4B_6O_{13}$, displays excellent crystallinity and high mechanical hardness [5]. Moreover, it also exhibits high optical transmission capacity, which makes it relevant for luminescence applications [5, 7]. For instance, Liang Pan et al. [3] synthesized $Zn_4B_6O_{13}$ and Eu^{3+}/Tb^{3+} single-doped $Zn_4B_6O_{13}$ phosphors for w-LED applications. Zhao et al. [5] prepared multimodal emission in Tb^{3+}/Yb^{3+} doped $Zn_4B_6O_{13}$ for application in information encryption and Anti-counterfeiting.

It is well known that rare earth ions show stable emissions resulting from the f-f electron transitions, which make them suitable to be used as luminescent activators [5, 8, 9]. Eu^{3+} is one of the most investigated RE ions and is considered the main RE ion that achieves red light emission, which is important for improving the red-light component [10]. Eu^{3+} ions are essential for light-emitting phosphors and versatile display applications when excited with a wavelength in the UV region [11]. The most prominent emission peak normally observed at 611 nm which is due to the electric dipole transition $^5D_0 \rightarrow ^7F_2$ transition of Eu^{3+} ions [11, 12]. To the best of our knowledge, a comparative study within the metal ions of different oxidation states ranging from +1 to +4 incorporated into Eu^{3+} doped $Zn_4B_6O_{13}$ lattice has not been studied. In this work, we aim to improve the luminescence properties of this important material by incorporating metal ions of different oxidation states M^{x+} (x = 1 to 4).

2 Experimental procedure

2.1 Synthesis

All the investigated phosphors were prepared by combustion synthesis using urea as a fuel. Firstly, the raw materials $Zn(NO_3)_26H_2O$(99%), H_3BO_3(99.5%), $Eu(NO_3)_36H_2O$(99.99%), $NaNO_3$(99.5%), $Ca(NO_3)_24H_2O$(99%), $Bi(NO_3)_35H_2O$(98%), and $MnCl_24H_2O$(98%) were accurately weighed according to the stoichiometric calculations for $Zn_4B_6O_{13}$, $Zn_4B_6O_{13}$:(2%)Eu^{3+}, and $Zn_4B_6O_{13}$: (2%)M^{x+}/(2%)Eu^{3+} samples. The weighed materials were transferred to the beaker and dissolved in 60 ml of De-ionized water. Then the mixture was stirred for about 10 min until a clear solution was formed. Then urea was added as a fuel and continue to stir for 20 min. The resulting mixture was then transferred into a crucible and placed in a furnace at 600 °C. The furnace was left to cool at room temperature. The powder samples were then ground and annealed at 900 °C for 1 hours. Finally, the annealed mass was thoroughly ground using a mortar and pestle and were taken for characterization.

2.2 Characterization

The XRD patterns of the prepared materials were performed by Bruker D8 Advanced X-ray diffractometer with Cu-Kα radiation (λ = 1.54 Å). The morphology and the elemental analysis were tested by JOEL JSM-7401 SEM coupled with EDS for elemental composition. Reflectance and band gap information was obtained through the diffuse reflectance spectra using Perkin-Elmer Lambda 950 UV-Vis spectrometer measured at room temperature. PL excitation and emission scans were carried using Cary Eclipse spectrometer with 150W xenon lamp as an excitation source. For chromaticity co-ordinates, the 1931 CIE software was employed.

3 Results and discussion

3.1 X-Ray diffraction analysis

Figure 1 (a) depicts the XRD patten comparison of $Zn_4B_6O_{13}$: Eu^{3+}, $Zn_4B_6O_{13}$: Eu^{3+} doped with metal ion of different oxidation states M^{x+} (x = 1 to 4), and the undoped $Zn_4B_6O_{13}$. The concentration of Eu^{3+} and M^{x+} were both kept at 2 mol%. The XRD pattens of the undoped $Zn_4B_6O_{13}$ host material reveal the formation of a cubic crystallography system of space group I-43m, which is completely consistent with standard card PDF# 01-080-7675 ($Zn_4B_6O_{13}$ structure) and previous studies [5, 1]. Doping with Eu^{3+} shows the presence of superlattices diffraction peaks at angle 2θ of 29.1°, 38°, 46°, 48°, and 52° corresponding to (211), (310), (321), (400), and (330) planes of $Zn_4B_6O_{13}$ structure, respectively. This shows complete incorporation of Eu^{3+} into $Zn_4B_6O_{13}$ matrix. Further incorporating with metal ions of different oxidation state (M^{x+}, x = 1 to 3) did not alter the crystal structure of the $Zn_4B_6O_{13}$ material. No further peaks of impurity phases of Na^+, Ca^{2+}, or Bi^{3+} were detected. This shows that the materials also adopt the cubic ordered Zinc metaborate lattice structure. All samples show sharp intense XRD peaks which reveal that the prepared materials are of high well-ordered crystallinity [1]. From all prepared materials, no characteristic peaks from other forms of borate such as ZnB_4O_7, ZnB_2O_4, or $Zn_3(BO_3)_2$ were observed [4, 13]. The XRD results confirm that the crystalline $Z_4B_6O_{13}$ with Eu^{3+} and M^{x+} (x = 1 to 3) doping could be achieved by the mentioned combustion synthesis sample preparation conditions.In contrast, incorporating the Mn^{4+} ion resulted in extra peak appearing in the $Z_4B_6O_{13}$. XRD patterns. **Figure 1 (b)** shows magnified 2θ region (28°-30°) of the most prominent peak (29.1°). A noticeable shift to higher 2θ values is mostly observed from the Ca^{2+} doped $Zn_4B_6O_{13}$:Eu^{3+} sample and this may be due to the difference in the ionic radii of Ca^{2+} (0.99Å) [14] and Zn^{2+}(0.74 Å) [3]. **Figure 2.** Shows the XRD patten of $Zn_4B_6O_{13}$:Mn, $Zn_4B_6O_{13}$:Mn/Eu^{3+}, and $Zn_4B_6O_{13}$:Eu^{3+} on the magnified region of 2θ angles (20° – 36°). From the enlarged XRD (**Figure 2 (b)**), there is a clear observation of the secondary structure. This can be identified by the extra peaks marked with an

asterisk (*) that does not belong to the $Zn_4B_6O_{13}$ cubic crystal structure profile. As observed from the Eu^{3+} and Mn^{4+} singly doped $Zn_4B_6O_{13}$ materials, it is evident that the incorporation of the Mn^{4+} ions into $Zn_4B_6O_{13}$ is the one that causes impurities into the structure and not the incorporation of Eu^{3+}.

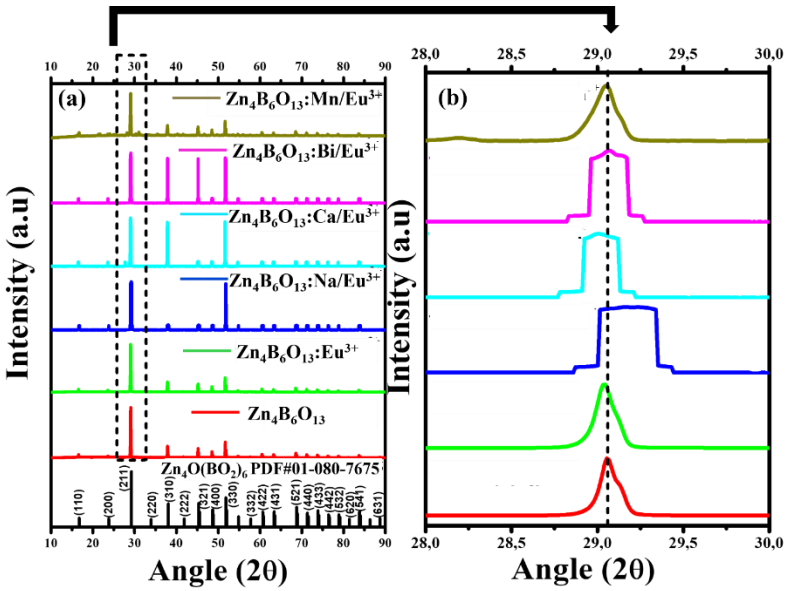

Figure 1: (a) Structural analysis and **(b)** magnified 2θ (28°-30°) of $Zn_4B_6O_{13}$: Eu^{3+} doped with metal ions of different oxidation state M^{x+} (x = 1 to 4).

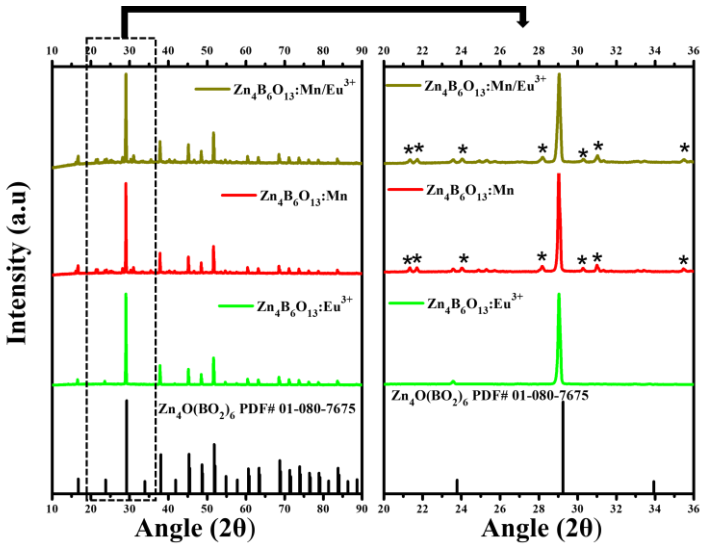

Figure 2: XRD patterns of **(a)** $Zn_4B_6O_{13}$:Eu^{3+}, $Zn_4B_6O_{13}$:Mn, and $Zn_4B_6O_{13}$:$Mn/Eu^{3+}$and **(b)** Enlarged XRD pattern (2θ: 20°-36°).

3.2 Morphological studies and elemental composition

The SEM images and corresponding EDS spectra of undoped $Zn_4B_6O_{13}$, Eu^{3+} doped $Zn_4B_6O_{13}$, monovalent (Na^+), and divalent (Ca^+) doped $Zn_4B_6O_{13}$:Eu^{3+} phosphors are displayed in **Figure 3**. From the insert, SEM images in **Figure 3 (a)** and **(b)** for undoped $Zn_4B_6O_{13}$ and $Zn_4B_6O_{13}$:Eu^{3+} materials respectively, the observed surface structures are of similar nature, however, more agglomeration is seen from the undoped $Zn_4B_6O_{13}$ sample. Both materials are characterized by irregular polyhedron morphology with smooth surfaces and sharp edges. The observed surface structures are characteristic of the $Zn_4B_6O_{13}$ cubic structure and agree with previous studies [3,

15]. The Na^{+} doped $Zn_4B_6O_{13}:Eu^{3+}$ (**Figure 3 (c)**) sample shows more agglomeration with deposits of irregular shapes on the surfaces, and the Ca^{2+} doped $Zn_4B_6O_{13}:Eu^{3+}$ sample (**Figure 3 (d)** insert) shows voids with different particle sizes across the surface. However, the characteristic polyhedron morphology of $Zn_4B_6O_{13}$ is maintained in both materials [3]. The EDS spectra of **Figure 3 (a)** and **(b)** correspond to undoped $Zn_4B_6O_{13}$ and $Zn_4B_6O_{13}:Eu^{3+}$ materials, respectively. The Eu element peaks are only observed from the Eu^{3+} doped $Zn_4B_6O_{13}$ sample, and all other expected elements are present in both samples with no extra impurity elements peaks. This confirms that Eu^{3+} ion was successfully doped into $Zn_4B_6O_{13}$. The existence of elements, Zn, B, O, Na, and Eu in $Zn_4B_6O_{13}:Na/Eu^{3+}$ and Zn, B, O, Ca, and Eu in $Zn_4B_6O_{13}:Ca/Eu^{3+}$ are confirmed by the EDS, **Figure 3 (c)** and **(d)**, respectively. The presence of C and Ir is due to carbon tape coating during measurements.

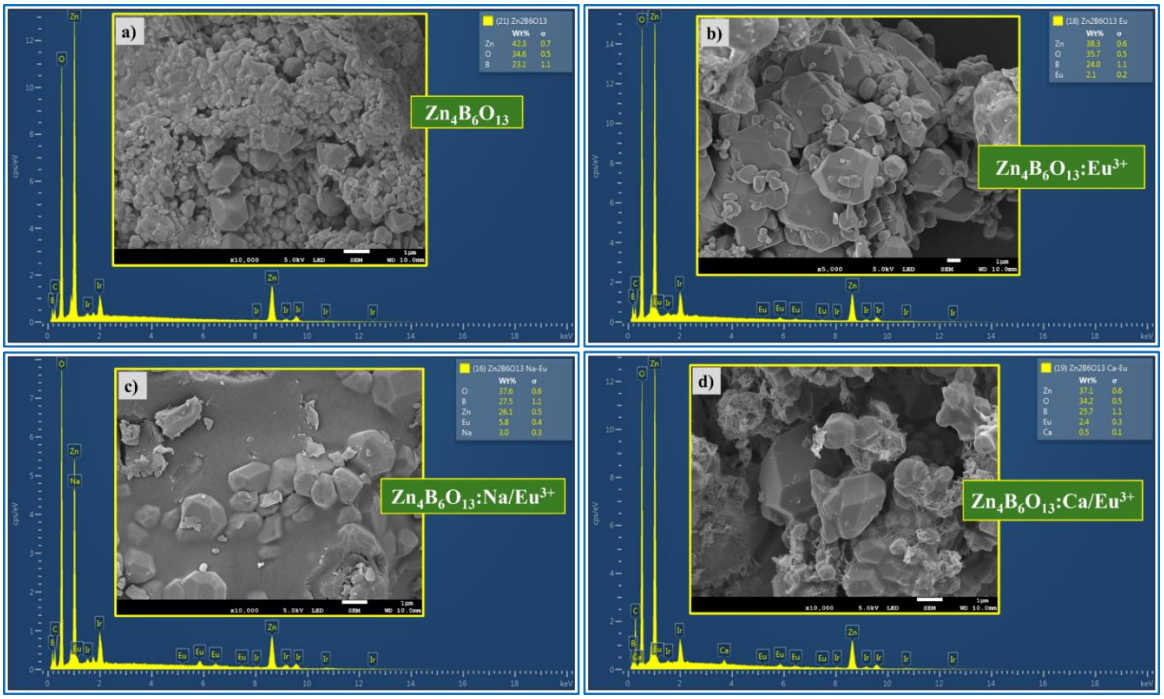

Figure 3: EDS spectra and inserts SEM images of **a)** $Zn_4B_6O_{13}$ host, **b)** $Zn_4B_6O_{13}:Eu^{3+}$, **c)** $Zn_4B_6O_{13}:Na/Eu^{3+}$ host, and **d)** $Zn_4B_6O_{13}:Ca/Eu^{3+}$.

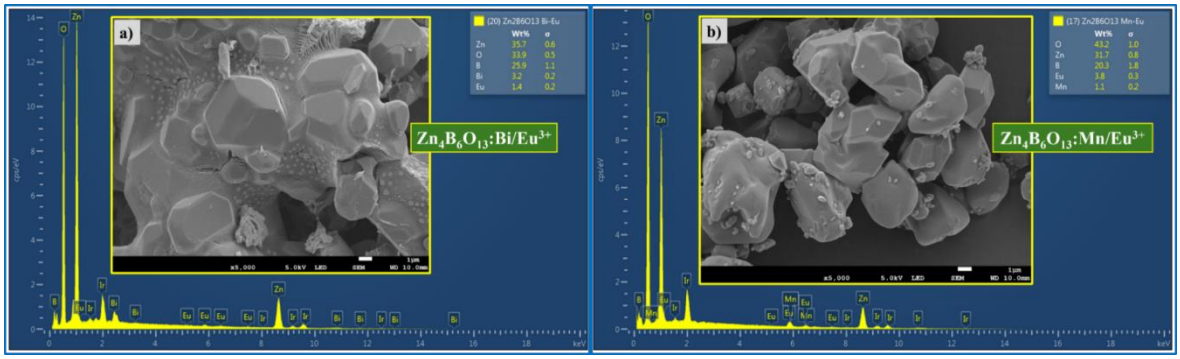

Figure 4: EDS spectra and inserts SEM images of **a)** $Zn_4B_6O_{13}:Bi/Eu^{3+}$, **b)** $Zn_4B_6O_{13}:Mn/Eu^{3+}$

Figure 4 presents the EDS spectra and SEM images (inserts) of **(a)** $Zn_4B_6O_{13}:Bi/Eu^{3+}$ and **(b)** $Zn_4B_6O_{13}:Mn/Eu^{3+}$. The $Zn_4B_6O_{13}:Bi/Eu^{3+}$ sample shows distribution of polyhedral surfaces of different sizes on the material's surface. The $Zn_4B_6O_{13}:Mn/Eu^{3+}$ material is characterized by combination of both solid polyhedron and round morphology with some particle deposits on the surfaces. This may be due to the formation of secondary phase structure as discussed earlier in the XRD analysis. The microstructural characteristics of materials may

influence the PL properties of phosphor materials [16]. Respective EDS diagrams confirm the presence of all elements with no impurities.

3.3 Photoluminescence study of $Zn_4B_6O_{13}:Eu^{3+}/M^{x+}$

Figure 5 depicts the **(a)** Excitation scan, **(b)** PL emission scan and **(c)** CIE spectra for $Zn_4B_6O_{13}:M^{x+}/Eu^{3+}$ materials. From the excitation scan (**Figure 5 (a)**) under 614 nm emission wavelength, Eu^{3+} excitation peak profile is observed from all the prepared materials [3]. These excitation bands are observed at wavelengths of 362 , 381, 395, and 465 nm corresponding to $^7F_0 \rightarrow {}^5D_4$, $^7F_0 \rightarrow {}^5L_7$, $^7F_0 \rightarrow {}^5L_6$, and $^7F_0 \rightarrow {}^5D_2$ transitions of Eu^{3+} ions, respectively [3, 11]. Amongst these excitation wavelengths of Eu^{3+}, the highest excitation peak is at 395 nm. A broad absorption band between 200 – 300 nm is ascribed to charge transfer band (CTB) due to ligand to metal transition (O^{2-} - Eu^{3+}) [12, 17]. The PL emission scan was caried out under the prominent excitation wavelength of 395 nm of Eu^{3+} (**Figure 5 (b)**). All samples show the Eu^{3+} PL spectral bands at wavelengths 580 nm, 592 nm, 614 nm, 654 nm, and 704 nm due to $^5D_0 \rightarrow {}^7F_0$, $^5D_0 \rightarrow {}^7F_1$, $^5D_0 \rightarrow {}^7F_2$, $^5D_0 \rightarrow {}^7F_3$, and $^5D_0 \rightarrow {}^7F_4$, transitions, respectively [12, 11, 18]. The hypersensitive electric dipole transition ($^5D_0 \rightarrow {}^7F_2$) is mostly favored compared to the magnetic dipole transition which indicates that the Eu^{3+} occupies the low symmetric sites in the crystal lattice [3, 19]. The effect of the metal ions of different oxidation states on the peak intensity is greater, and the order of the light intensity from strong to weak is $Zn_4B_6O_{13}:Bi/Eu^{3+}$ > $Zn_4B_6O_{13}:Ca/Eu^{3+}$ > $Zn_4B_6O_{13}:Na/Eu^{3+}$ > $Zn_4B_6O_{13}:Eu^{3+}$ > $Zn_4B_6O_{13}:Mn/Eu^{3+}$. All the M^{x+} samples show high intensity compared to Eu^{3+} singly doped $Zn_4B_6O_{13}$ material except for the Mn^{4+} doped sample having the lowest intensity and this may be due to the secondary structure introduced by incorporating with Mn^{4+} ions. Compared to the $Zn_4B_6O_{13}:Eu^{3+}$ material, the luminescence intensity increase is 4.9, 4.2, and 3.5 times for $Zn_4B_6O_{13}:Bi/Eu^{3+}$, $Zn_4B_6O_{13}:Ca/Eu^{3+}$, and $Zn_4B_6O_{13}:Na/Eu^{3+}$ phosphor, respectively, which significantly enhance the luminescence performance. **Figure 5 (c)** represents the CIE diagram for the prepared materials. The $Zn_4B_6O_{13}:Eu^{3+}$ shows adjustable color light from reddish-orange to red emission with incorporation of metal ions of different oxidation states M^{x+} (x =1 to 3).

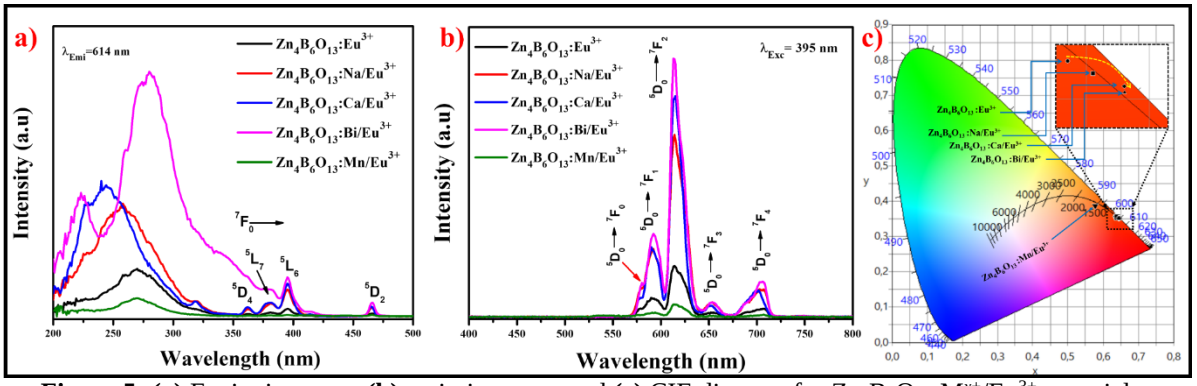

Figure 5: (a) Excitation scan, **(b)** emission scan, and **(c)** CIE diagram for $Zn_4B_6O_{13}:M^{x+}/Eu^{3+}$ materials.

4 Conclusion

XRD results confirm the successful synthesis of $Zn_4B_6O_{13}:M^{x+}/Eu^{3+}$ and the material compositions are further confirmed by EDS results. The SEM images confirm the characteristic polyhedron morphology of the $Zn_4B_6O_{13}$ cubic crystal structure. PL comparative study of the influence of metal ions of different oxidation states M^{x+} (x =1 to 4) on the emission properties of Eu^{3+} doped $Zn_4B_6O_{13}$ shows that the order of PL intensity from strong to weak is $Zn_4B_6O_{13}:Bi/Eu^{3+}$ > $Zn_4B_6O_{13}:Ca/Eu^{3+}$ > $Zn_4B_6O_{13}:Na/Eu^{3+}$ > $Zn_4B_6O_{13}:Eu^{3+}$ > $Zn_4B_6O_{13}:Mn/Eu^{3+}$. This suggests that Bi^{3+} can improve the absorption bands and limit the nonradiative transitions, which further enhance the luminescence properties of the prepared phosphors. The incorporation of metal ions can improve the color purity of the material by shifting to deeper red emission of Eu^{3+}. The results suggest that these materials may be viable option for UV and LED chips and key element in fabrication of wLEDs.

References

[1] Liu, Y., Li, C., Din, M.A.U., Tang, L., Lin, Y. and Cheng, N., 2022. Optical properties of Eu^{3+}/Pr^{3+} doped $Zn_4O(BO_2)_6$ synthesized by solid-state reaction. *Ceramics International*, *48*(11), pp.15737-15747.

[2] Yang, Y., Jiang, X., Gong, P., Molokeev, M.S., Li, X., Li, Y., Wu, X., Wu, Y. and Lin, Z., 2017. High mechanical strength in $Zn_4B_6O_{13}$ with an unique sodalite-cage structure. *RSC Advances*, *7*(4), pp.2038-2043.

[3] Liang, P., Mingzhen, W.A.N.G. and Zhihong, L.I.U., 2017. Synthesis and spectroscopic studies of $Zn_4B_6O_{13}$ and Eu/Tb single-doped $Zn_4B_6O_{13}$ phosphors. *Journal of Rare Earths*, *35*(5), pp.441-445.

[4] Lian, W.L., Liang, P. and Liu, Z.H., 2020. Controllable hydrothermal synthesis and morphology evolution of $Zn_4B_6O_{13}$:Tb/Eu phosphors with tunable luminescent properties. *Advanced Powder Technology*, *31*(4), pp.1633-1642.

[5] Zhao, S., Wang, Z., Ma, Z., Fan, F. and Liu, W., 2020. Achieving multimodal emission in $Zn_4B_6O_{13}$:Tb^{3+}, Yb^{3+} for information encryption and anti-counterfeiting. *Inorganic Chemistry*, *59*(21), pp.15681-15689.

[6] Wang, P.D., Jia, Z.Y., Zhong, Y.H., Mei, H.Y., Li, C.M. and Cheng, N.P., 2018. Effect of pressure on the elastic properties and optoelectronic behavior of $Zn_4B_6O_{13}$:First-principles investigation. *Chinese Physics B*, *27*(5), p.057101.

[7] Alemi, A., Mohseni, N., Dolatyari, M. and Bakhtiari, A., 2012. New Method for Synthesis of Zinc Metaborate $Zn_4B_6O_{13}$ Crystals via Sol-Gel Process and Investigation of DFT Calculations. *Int. J. Bio-Inorg. Hybd. Nanomat*, *1*(2), pp.79-86.

[8] Chen, W., Ouyang, Y., Mo, M., Zhang, H. and Su, Q., 2021. Observation of energy transfer from Eu^{2+} to Eu^{3+} and tunable luminescence in phosphors YF_3:Eu prepared by hydrothermal method. *Journal of Luminescence*, *229*, p.117672.

[9] Dereń, P.J., Stefanska, D., Ptak, M. and Wisniewski, P., 2021. Method to measure the degree of reduction of Eu^{3+} to Eu^{2+}: how anion and cation vacancies influence the degree of reduction. *The Journal of Physical Chemistry C*, *125*(44), pp.24505-24514.

[10] Li, X., Yang, C., Liu, Q., Wang, X. and Mi, X., 2020. Enhancement of luminescence properties of SrAl2Si2O8: Eu^{3+} red phosphor. *Ceramics International*, *46*(11), pp.17376-17382.

[11] Verma, N., Michalska-Domańska, M., Ram, T., Kaur, J., Misra, A.K., Dubey, V., Dubey, N., Tiwari, K. and Rao, M.C., 2023. Optimizing the luminescence efficiency of an europium (Eu^{3+}) doped SrY_2O_4 phosphor for flexible display and lighting applications. *RSC advances*, *13*(29), pp.20217-20228.

[12] Cao, R., Huang, Z., Lan, B., Li, L., Yi, X., Luo, Z., Liao, C. and Wang, J., 2022. Adjustable luminescence properties of Eu^{3+} and Bi^{3+} codoped $Ca_3Zn_3Te_2O_{12}$ phosphor. *Materials Research Bulletin*, *152*, p.111851.

[13] Kucuk, N., Kaynar, Ü.H., Akca, S., Alajlani, Y., Yin, L., Wang, Y., Guinea, J.G., Bulcar, K., Dogan, T., Karabulut, Y.Ü.K.S.E.L. and Ayvacikli, M.E.H.M.E.T., 2020. Enhancing the blue luminescence behaviour of the Li co-doped novel phosphor ZnB_2O_4: Tm^{3+}. *Journal of Alloys and Compounds*, *838*, p.155587.

[14] Dwivedi, A., Srivastava, M., Dwivedi, A., Srivastava, A., Mishra, A. and Srivastava, S.K., 2022. Synthesis and enhanced photoluminescence properties of red emitting divalent ion (Ca^{2+}) doped Eu: Y_2O_3 nanophosphors for optoelectronic applications. *Journal of Rare Earths*, *40*(8), pp.1187-1198.

[15] Maleho, E.T., 2022. *Investigation of the photoluminescence studies of ZnO: RE^{3+} (where RE= Dy, Sm and Sm/Dy) nanophosphors via different anionic group (BO_3^{3-}, PO_4^{2-} and SO_4^{2-}) substitutions* (Doctoral dissertation, University of Johannesburg).

[16] Jasira, S.V., Veena, V.P., Shilpa, C.K., Ancy, S.S. and Nissamudeen, K.M., 2025. Innovative white light emission from europium-doped barium cerate: A comprehensive study from structural analysis to emission spectroscopy. *Journal of Molecular Structure*, p.142547.

[17] Li, Y., Zhang, J., Zhang, X., Luo, Y., Lu, S., Ren, X., Wang, X., Sun, L. and Yan, C., 2009. Luminescent properties in relation to controllable phase and morphology of $LuBO_3$: Eu^{3+} nano/microcrystals synthesized by hydrothermal approach. *Chemistry of Materials*, *21*(3), pp.468-475.

[18] Klement, R., Drdlíková, K., Kachlík, M., Drdlík, D., Galusek, D. and Maca, K., 2021. Photoluminescence and optical properties of Eu^{3+}/Eu^{2+}-doped transparent Al_2O_3 ceramics. *Journal of the european ceramic society*, *41*(9), pp.4896-4906.

[19] Bispo-Jr, A.G., Saraiva, L.F., Lima, S.A., Pires, A.M. and Davolos, M.R., 2021. Recent prospects on phosphor-converted LEDs for lighting, displays, phototherapy, and indoor farming. *Journal of Luminescence*, *237*, p.118167.